Transport of Kr^{35+} inner-shells through solid carbon foils*

D. Vernhet[1+], C. Fourment[1], E. Lamour[1], J-P. Rozet[1],B. Gervais[2], L. J. Dubé[4]
F. Martín[3], T. Minami[5], C. O. Reinhold[5,6], M. Seliger[7], J. Burgdörfer[7,5]

[1]GPS, CNRS UMR 75-88, Universités Paris 7 et Paris 6, 75251 Paris Cedex 05, France
[2]CIRIL, CEA-ISMRA-CNRS UMR 66-37, 14070 Caen, Cedex, France
[3]Departamento de Química, Universidad Autónoma de Madrid, 28049-Madrid, Spain
[4]Département de Physique, Université Laval, Cité Universitaire, Québec G1K 7P4, Canada
[5]Department of Physics, University of Tennessee, Knoxville, TN 37996, USA
[6]Physics Division, Oak Ridge National Laboratory, Oak Ridge, TN 37831-6373, USA
[7]Institute for Theoretical Physics, Vienna University of Technology, A 1040 Vienna, Austria

Abstract: New experimental data on the transport of Kr^{35+} inner-shells initially populated either by capture or by excitation processes are presented. Absolute Lyman ($np \rightarrow 1s$) intensities, directly related to the np state populations, as well as $3l_j$ substate populations have been determined over a range of carbon target thickness allowing to study the transport from single collision conditions to equilibrium. Results are compared with predictions of different transport simulations which take into account multiple collisions, the strong target polarization induced by the incoming HCI (the wake field), and radiative decay. Very good agreement is found between theory and experiment for the np populations up to n=5 where induced wake mixing becomes visible. The simulations also explain the behavior of the $3l_j$ populations of Kr^{35+} which exhibit a strong sensitivity to the presence of radiative decay during transport and the effective value of the wake field.

PACS numbers: 34.50.Fa, 39.30.+w, 34.10.+x
9/1/00

* Experiment performed at GANIL-Caen

1. Introduction

Transport of electrons in excited states of fast ions through solids as a probe of ion-solid interactions is a subject of current investigation. Experimentally, the evolution of Rydberg and core states has been determined for different target thicknesses, from single collision conditions to equilibrium of populations using x-ray spectroscopy [1, 2]. In parallel, quantum and classical theories for this problem have been developed trying to incorporate various aspects of the interaction [2-4]. Namely, *the multiple collisions* that projectile electrons suffer with particles in the solid, the strong *target polarization* induced by the incoming HCI (the wake field), and the *radiative decay* of the ion. Early simulations focused on the time evolution of the occupation probabilities of excited states and is known as the *rate equation model* [1, 5]. Recently, more elaborate simulations have been developed to study the evolution of the density matrix [2,4,7]. A description involving only multiple collisions reproduces well the behavior of nl populations of Rydberg projectile excited states but fails for the inner shells [1, 6]. This is partly due to the fact that the interplay between multiple scattering and dynamical screening can enhance the population of high-l states [3]. Furthermore, np and $3l_j$ populations exhibit strong sensitivity to the effective value of the electric field for a given nl state and to coherences of the density matrix resulting from a few collisional processes: electron capture by HCIs or excitation from the ground state of HCIs [3, 7].

Thus far, only excited states initially populated by ***capture*** have been studied. As an example for such a system we present results for 33.2 MeV/u Kr^{36+} ions colliding with amorphous carbon foils. In addition, we present new results for 60 MeV/u Kr^{35+} ions, where the initial state of the ion prior to transport is given by the ***ground state***.

We study the population dynamics of the excited states of the Kr^{35+} ion. Experimental information on these populations is extracted from Lyman lines *(np→1s*, with $n \leq 5$*)* and the Balmer αlines ($3l_j \rightarrow 2l'_{j'}$) from the Kr^{35+} ion. Atomic units are used throughout unless indicated otherwise.

2. Experiment

Both experiments with Kr^{36+} and Kr^{35+} projectiles at 33.2 MeV/u and 60 MeV/u, respectively, have been performed at GANIL (Grand Accélérateur National d'Ions Lourds) on the LISE (Ligne d'Ions Super Epluchés) facility. The complete experimental set-up has been already described in detail elsewhere [1,2,6]. Here we summarize its main characteristics. Beams are directed onto self-supported amorphous carbon foils with measured thicknesses and purity [6]. The foils can be tilted to change the effective transport thickness. Foil thicknesses are changed from 3 to 220 $\mu g/cm^2$ to study the ion transport from near single collision conditions to equilibrium. Lyman (np→1s) intensities are measured for $n \leq 5$ by a Si (Li) detector as a function of target thickness to investigate the evolution of *np* state populations [2,3]. Balmer α lines are also measured using high-resolution high-transmission Bragg-crystal spectrometers. From the intensity of photons emitted, directly measured, relative state populations of $3p_{1/2}$ and $3s_{1/2}$ as well as $3d_{3/2}$ and $3d5_{/2}$ are deduced using formulas in [6] transition probabilities in [8]. Each detection system is placed at a specific angle with respect to the beam direction to insure a polarization-insensitivity of the measurements.

3. Theoretical simulations

The starting point of any quantum description of the ion-solid interaction is the reduced density matrix σ describing the state of the electron in the ion. Ideally, the

time evolution of the electron is governed by a quantum Liouville equation (QLE) containing dissipative and non-dissipative terms. Dissipative terms describe the interaction with the environment and include multiple collisions and radiative decay. Non-dissipative terms describe the free time evolution of the electron in the screened Coulomb field of the ion (i.e. the wake field). Our theoretical simulations try to solve the QLE by different methods and using various approximations for the dissipative terms. The first model presented in this section directly solves the QLE as a matrix equation but using a limited set of dissipative couplings. The second model attempts to solve the QLE using a Monte Carlo approach which reduces the problem to a microscopic quantum Langevin equation.

3.1 *Master equations approach (MEA)*

Within a given subspace, the time evolution of the density matrix is obtained by solving a set of coupled differential equations that may succinctly be written as [2,7]

$$\frac{d}{dt}\sigma_{ab}(t) = \left\{ i\omega_s(a,b)\ \left[\sigma_{aa}(t) - \sigma_{bb}(t)\right] \right\} - i\omega_{ab}\sigma_{ab}(t) - \frac{\Gamma_{ab}}{2}\sigma_{ab}(t) \qquad \textit{for } a \neq b \tag{1}$$

$$\frac{d}{dt}\sigma_{aa}(t) = i \sum_{c} \omega_s(c,a)\left[\sigma_{ac}(t) - \sigma_{ca}(t)\right] + \sum_{c \neq a} \left[\Gamma_{ca}\sigma_{cc}(t) - \Gamma_{ac}\sigma_{aa}(t)\right], \tag{2}$$

where the first term in (1) denotes the coupling induced by the wake field, while the second term includes radiative and collisional damping. Equation (2) includes radiative and collisional processes (1st term) as well as the coupling among coherences (2nd term). In equations (1) and (2), ω_s is the Stark mixing element, ω_{ab} is the Bohr frequency between states *a* and *b,* and the Γ_{ij} are the widths corresponding to radiative and collisional processes. All the transition rates are calculated ab-initio

and we account for all the cross sections of the processes involved during transport. More specifically, we first calculate cross sections in a $n\mathrm{l}_j m_j$ basis for capture and ionization processes as well as for the inter-shell and intra-shell excitation. We also take into account the radiative decay as a competitive process occurring during the transport. We however neglect many-body excitations of the solid on the collisional cross sections. In addition, Eq. (1) neglects the collisional couplings between $\sigma_{a,b}$ with density matrix elements involving states *c* other than *a* or *b*. For this reason, the simulations is not directly started from the ground state of Kr^{35+}. Instead, the initial density matrix represents a coherent superposition of excited states, which is calculated as follows. In the case of $Kr^{36+}\rightarrow C$ at 33.2 MeV/u, the continuum distorted wave (CDW) approximation is used to describe the initial density matrix resulting from a capture process while in the case of $Kr^{35+}\rightarrow C$ at 60 MeV/u the initial density matrix ($\sigma\ (t=0)$) resulting from excitation from the ground state is calculated using a plane-wave first Born approximation (PWBA) or close coupling (CC) calculations [9]. Convergence is usually reached for calculations involving all the substates of the n=1-6 shells (changes when going from n_{max}=5 to 6 do not exceed 2%). The hydrogen-like ion transport through solids is treated "separately" and permits us to easily gauge the sensitivity of the data to the initial coherence terms or to the effective electric field value induced by the wake. Furthermore, we can examine the influence of selectively switching "on/off" the wake effect state by state.

3.2 *Quantum transport theory (QTT)*

In this model, we solve the QLE for the reduced density matrix using a Monte Carlo approach which reduces the dynamics of the electron to a microscopic quantum

Langevin equation. The reduced density operator $\sigma(t)$ is calculated in terms of quantum trajectories $\Psi_u(t)$ as

$$\sigma(t) \ldots \frac{1}{K} \sum_{u=1}^{K} \left|\Psi_u(t)\right\rangle\left\langle\Psi_u(t)\right| \tag{3}$$

where K is the number of trajectories whose time evolution is governed by the Langevin equation

$$i\frac{d}{dt}\left|\Psi_u(t)\right\rangle = \left\{H_{atom} + V_{stoc}(t)\right\}\left|\Psi_u(t)\right\rangle, \tag{4}$$

In this equation, the atomic Hamiltonian $H_{atom} \ldots p^2/2 + V(r)$ where $V(r)$ includes the Coulomb interaction with the nucleus and the wake field. The stochastic potential $V_{stoc}(t)$ in Eq. (4) accounts for multiple collisions [4] and the interaction with the electromagnetic field (radiative decay). The time evolution of each quantum trajectory can be rewritten in terms of the time evolution operator.

$$\left|\Psi_u(t)\right\rangle = U(t)\left|\Psi_u(0)\right\rangle$$

$$U(t) \ldots U_{atom}(t - t_k) \prod_{k=1}^{K} U_{stoc}(t_k) U_{atom}(t_k - t_{k-1}) \qquad (t_0 \ldots 0)$$

Here, $U_{atom}(t) \ldots exp(-i H_{atom} t)$ denotes the free evolution between the sudden interactions with environment, which are described by $U_{stoc}(t)$. The times between interactions are chosen at random from the corresponding mean free paths for multiple collisions or radiative decay, which are calculated within first order perturbation theory. For multiple collisions, $U_{stoc}(t) = e^{i\Delta\vec{p}\vec{r}}$ where $\Delta\vec{p}$ is a collisional momentum transfer which is sampled at random from the differential inverse mean free path for carbon. The radiative decay from state *i* to *j* is described through $U_{stoc}(t)$ which transfers all the probability from *i* onto *j*. The effect of the

radiative decay is incorporated in this work for the first time within this quantum transport formalism and will be described in a forthcoming publication.

4. Results

4.1. *Absolute Lyman lines intensities*

The absolute Lyman line intensities per incident ion, at different target thicknesses, are presented in Fig. 1. The MEA results are in very good agreement with experimental data over the whole range of target thicknesses. The results in the figure indicate that transport effects (i.e. differences from calculations using only a binary ion-atom collision) increase rapidly with the n quantum number of the observed level. Moreover, multiple collisions represent the dominant source of transport effects. The Lyman lines intensity becomes sensitive to the wake field for n=4 and higher. Indeed, for n=2, the Stark mixing rate ω_s is very small owing to the Lamb-shift splitting between the $2s_{1/2}$ and $2p_{1/2}$ levels. For n=3 l-mixing due to the wake field vanishes since the $3s_{1/2}$-$3p_{1/2}$ and $3p_{3/2}$-$3d_{3/2}$ mixing somehow counterbalance each other (the observed total np population corresponds to a sum over j components).

4.2. *Line intensities emanating from $3l_j$ states*

The evolution of relative populations of $3l_j$ states is displayed in Fig.2. The large deviations from binary ion-atom collision results indicate that the $3l_j$ populations are quite sensitive to the transport process. In particular, the $3p_{1/2}/3s_{1/2}$ ratio is seen to increase very rapidly with foil thickness. This increase is a direct consequence of the

$3s_{1/2} - 3p_{1/2}$ mixing and the radiative decay of the atom during transport. Indeed, the $3p_{1/2}$ state decays much faster than the $3s_{1/2}$ state.

The results of the MEA in Fig.2 *a)* are in good agreement with experimental data indicating that the CDW initial density matrix and the effective electric field (deduced from the spatial extension of the wake field [7, 10]) seem to be accurate. Furthermore, subsequent collisional coherences, which are neglected in the MEA do not seem to play an important role. Indeed, the $3\,l\,j$ ratios are sensitive to coherence terms for very thin targets (≤50 μg/cm^2) for which Stark mixing is dominant whereas collisional processes become important for thicker foils.

For collisions of Kr^{35+}(1s) with carbon foils (Fig.2. *b)*) collisional coherences play an important role at least for the primary excitation process from the 1s state into other levels. Therefore, the initial density matrix in the MEA is the result of the first binary collision and is calculated using PWBA and CC calculations (both yield very similar results). In turn, the QTT treats collisional coherences explicitly and, therefore, the initial state corresponds to the 1s state of Kr^{35+}. The MEA and QTT predict similar tendencies but they do not completely agree with each other. Presently, these differences are being investigated.

5. Conclusion

In this paper, we briefly presented our new results on transport of hydrogen-like HCIs through solid foils at high velocity. We show that recent theoretical developments in quantum transport yield predictions for the evolution of inner-shell populations which are in reasonable agreement with experimental data. These models are able to explain the behavior of the photon intensities as a function of foil thickness in terms of a mixing process of the substates of the atom which is strongly

detailed presentation of the experimental data together with a complete discussion on the new theoretical developments will be given in forthcoming papers.

Acknowledgments

We thank the Univ. of Paris 6 et 7 for arranging a prolonged visit for LJD and for allowing us to organize a working meeting with BG, JB and COR. We also wish to extend our thanks to L. Adoui, A. Cassimi, J-P. Grandin, H. Rothard and C. Stéphan for their participation in the data acquisition. We acknowledge J-M. Ramillon from the CIRIL for his technical support and the exploitation staff of the GANIL for providing us assistance and high-quality beams. COR acknowledges support from the US DOE , OFES and OBES through ORNL, managed by UT-Battelle, LLC under contract DE-AC05-00OR22725. JB, TM, MS acknowledge support from the NSF and FWF (Austria).

References

[1] Vernhet, D., Rozet, J-P., Lamour, E., Gervais, B., Fourment, C., Dubé, L. J., Physica Scripta T **80A,** 83-86 (1999).
[2] Vernhet, D. *et al*, in The Physics of Electronic and Atomic Collisions, ed Y. Itikawa *et al*, AIP Conf. Proc. **500**, 666 (2000).
[3] Reinhold, C. O. *et al*, J. Phys. B **33**, L111-L117 (2000).
[4] Arbó, D.G., Reinhold, C. O., Yoshida, S., and Burgdörfer, J., Phys. Rev. A **60**, 1091 (1999).
[5] Nicolaï, P. *et al*, J. Phys. B. : At. Mol. Phys. **23**, 3609 (1990).
[6] Vernhet, D. *et al*, J. Phys. B **31**, 117-129 (1998).
[7] Rozet, J-P., Vernhet, D., Bailly-Despiney, I., Fourment, C., Dubé, L. J., J. Phys. B **32** 4677-4696 (1999).
[8] Pal'chikov, V. G., Physica Scripta **57,** 581-593 (1998).
[9] Martín, F., J. Phys B. : At. Mol. Phys.**32**, 501 (1999)
[10] Fuhr, J. D., Ponce, V. H., García de Abajo, F. J. and Echenique, P. M., Phys. Rev. B **57**, 9329 (1998)

Figure captions:

Fig. 1. Absolute Lyman lines intensity emitted by Kr^{35+} as a function of carbon target thickness for ***a)*** $Kr^{36+}\rightarrow C$ at 33.2 MeV/u and ***b)*** $Kr^{35+}\rightarrow C$ at 60 MeV/u. Experimental data are given by the symbols with error bars. The full and dashed lines correspond to the master equation predictions with the wake field "on" and off", respectively. The dash double dotted lines represent results of binary ion-atom collisions (i.e. without any transport)

Fig. 2. Evolution of the $3p_{1/2}/3s_{1/2}$ and $3d_{3/2}/3d_{5/2}$ relative populations with carbon target thickness for ***a)*** $Kr^{36+}\rightarrow C$ at 33.2 MeV/u and ***b)*** $Kr^{35+}\rightarrow C$ at 60 MeV/u. Experimental data are given by the symbols with error bars. The full and dashed lines correspond to the master equation predictions with the wake field "on" and "off", respectively and using initial density matrices obtained with CDW (***a***) and PWBA (***b***). The 2-state density matrix approach is shown, as an example, through a dash dotted line. The dotted curves correspond to the master equation model with CC initial condition (***b***). QTT calculations are denoted by triangles with wake field "on" and circles with wake field "off". Dashed double dotted lines represent results of binary ion-atom collision (i.e. without transport, which coincide to the collisional transport in the case of $3d_{3/2}/3d_{5/2}$ relative populations).

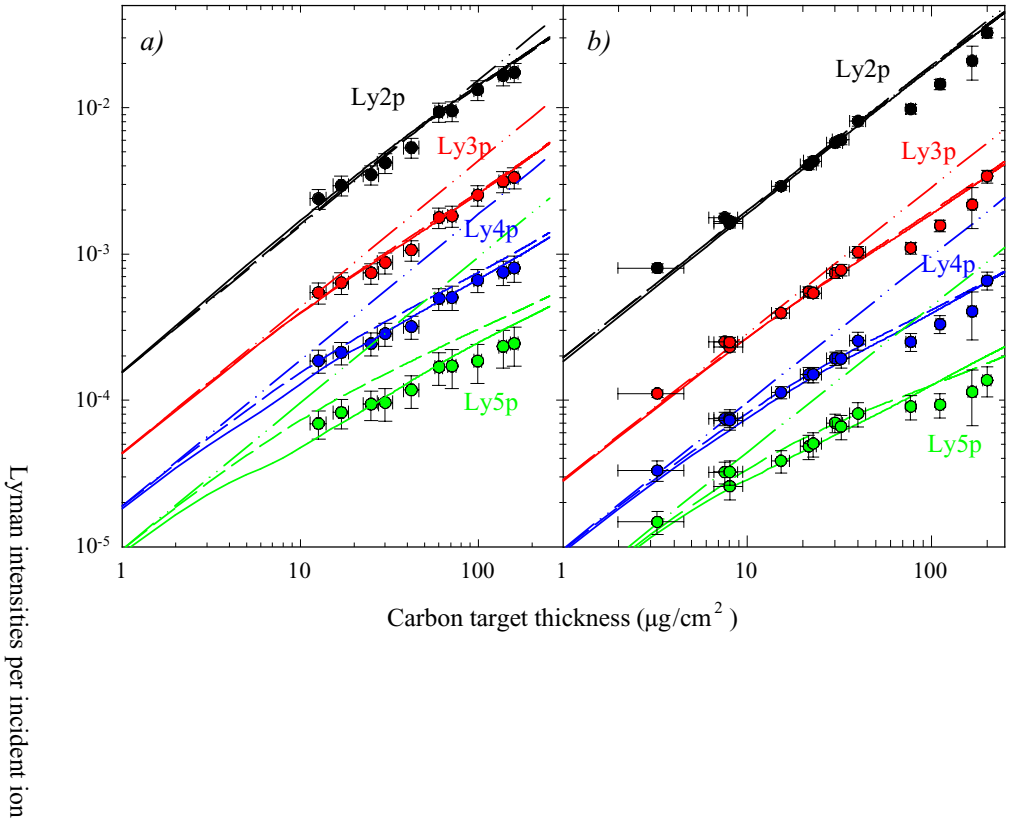
a)
b)
Ly2p
Ly3p
Ly4p
Ly5p
10^{-2}
10^{-3}
10^{-4}
10^{-5}
1
10
100
Carbon target thickness (μg/cm^2)
Lyman intensities per incident ion

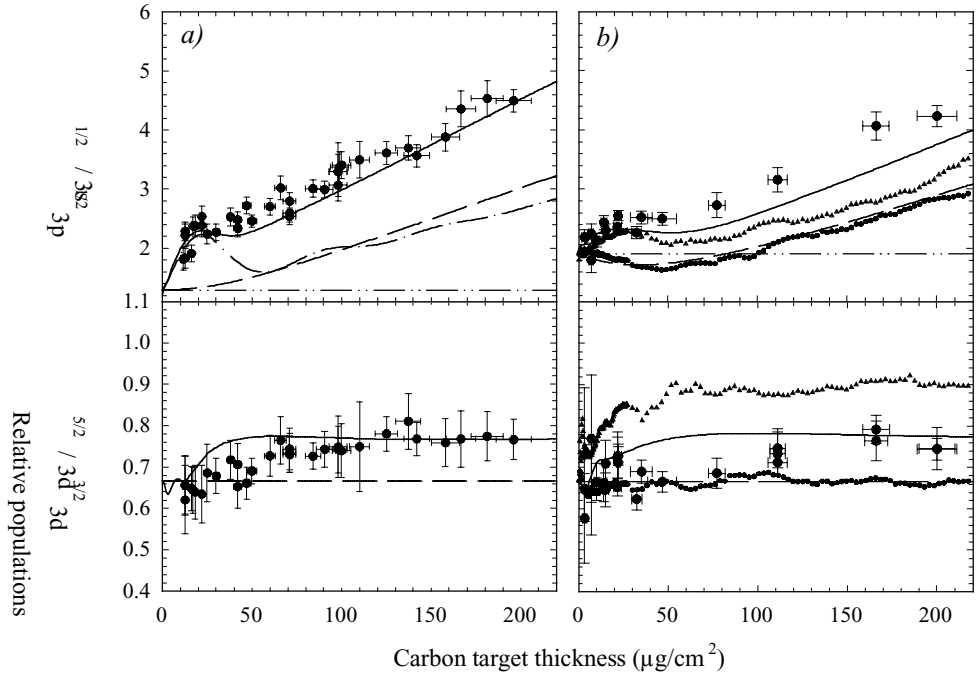
a)
b)
Relative populations
3p1/2 / 3s1/2
3d5/2 / 3d3/2
Carbon target thickness (μg/cm2)